EVIDENCE OF NORMAL FAULTING AND DIKE INTRUSION AT VALLES MARINERIS FROM PIT CRATER TOPOGRAPHY.

Chris H. Okubo[1] and Richard A. Schultz, Geomechanics–Rock Fracture Group, Department of Geological Sciences and Engineering /174, University of Nevada, Reno, NV, 89557-0138. [1]chriso@mines.unr.edu

INTRODUCTION: Pit crater chains (catenae) are among the most apparent structural features of Valles Marineris, second only to the wider and more contiguous chasmata. Numerous origins for these pit craters, as well as their role in the structural and geologic evolution of Valles Marineris, have been proposed based on photogeologic interpretations of satellite imagery. Models of pit crater formation on Mars commonly envisage an origin through stoping and collapse of surficial material into subsurface voids that are created by mode I opening displacements along tension fractures [1,2], igneous dikes [3,4], or dilational normal faults [5,6].

In this abstract, we evaluate the relative contributions of causative normal faulting and dike intrusion to the MOLA-based topography of pit crater chains at Valles Marineris. Our analysis reveals a dichotomy in causative processes across Valles Marineris. The topography of pit crater chains are consistent with origins by causative normal faulting as well as dike intrusion to the north of the Ius–Melas–Coprates chasmata, while causative normal faulting is the sole process identified to the south of this chasmata (Fig. 1).

FAULT– AND DIKE–RELATED TOPOGRAPHY: In order to establish distinguishing topographic characteristics of surface-breaking and buried normal faults and dikes, we construct a series of a boundary element models based on [7]. Following [8] we specify a crustal elastic modulus of 60 GPa, Poisson's ratio of 0.25, a rock mass friction angle of 30° with a cohesion of 0.5 MPa. Average crustal density is taken to be 2600 kg/m^3 and magma density is 2200 kg/m^3, with a the horizontal stress magnitude equal to two times the vertical stress (lithostatic load), assuming unsaturated conditions.

Figure 2 shows the characteristic dike- and fault-related topography predicted by our numerical models. The modeled normal faults have a constant dip of 60° and dikes are vertical. Further analysis (in a companion abstract [Okubo and Schultz, *this volume*]) shows that these characteristic dike and normal fault topographies are not significantly changed by natural variability in crustal strength and deformability. Normal fault-related topography is characteristically asymmetric, defined by footwall uplift and a rollover anticline within the subsiding hanging wall. Footwall uplift is characterized by concave-up topography, and the hanging wall anticline has a concave-down topography. Where two normal faults define a graben [8] footwall uplift is also predicted regardless of the relative lengths of the faults, and hanging wall anticlines are not predicted within the graben. Dike-related topography is characteristically symmetric, with ridges uplifted on either side of the surface projection of the dike. These paired ridges have concave-down topography and equal peak elevations.

ANALYSIS OF PIT CRATER CHAIN TOPOGRAPHY: In order to characterize the topography of pit crater chains at Valles Marineris, a series of MOLA based digital elevation models (DEMs) are created following the general procedure of [9] for a discontinuous-surface nearneighbor grid with a 200 pixel per degree (~296 m/pixel) resolution. DEM pixels are defined as the average value of coincident MOLA elevations, with no interpolation across pixels that lack MOLA data. Topographic profiles are extracted from these DEMs through contiguous MOLA-based pixels that span pit chain terminations, pit craters and septa between pit craters. These profiles are then compared to the characteristic normal fault and dike topographies. Profiles are classified as normal fault-related where there is a vertical offset and concave-up topography characteristic of footwall uplift across the pit crater chain. The profiles are classified as dike-related where there is a pair of concave-down ridges of sub-equal peak elevation on either side of the pit crater chain. Further, 'mixed-mode' topographies are also observed, where the paired concave-down ridges characteristic of dike-related topography have offset peak elevations (Fig. 3).

Figure 1 shows the distribution of pit crater chain topographies in the Valles Marineris region. Coprates catena is found to have normal fault-related topography along its entire length. Pit crater chains southwest of Ius chasma consistently show normal fault-related topography as well. Dike-related pit crater chain topography is observed north of the Ius–Melas–Coprates chasmata. Pure dike-related topography is common at

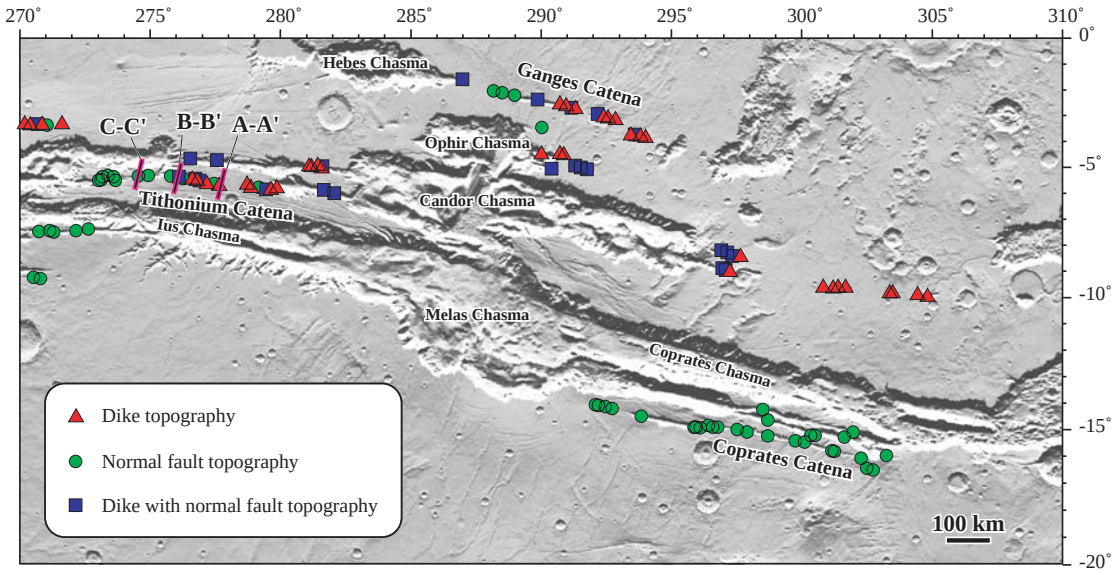

Figure 1. Distribution of dike, normal fault and mixed-mode topography across pit crater chains (catenae) in the Valles Marineris region based on analysis of discontinuous (non-interpolated) MOLA-based DEMs. Also shown are the locations for profiles in figure 3. Base map is shaded relief with illumination from the north.

and ahead of gradually-tapering pit crater chain terminations (e.g. east end of Ganges catena), while normal fault and mixed mode topographies are most common at the blunt terminations of these chains (e.g. west end of Ganges catena), or where the pit crater chains intersect the chasma (e.g. west end of Tithonium catena).

Our topographic analysis thus reveals two distinct causative processes for pit crater chain formation. Pit crater chains south of Ius and Coprates chasmata are shown to have formed above normal faults, consistent with the dilational normal fault mechanism suggested by [5,6]. Pit crater chains to the north of Ius–Melas–Coprates chasmata are found to have formed above dikes intruding radial to Tharsis, or above normal faults, or through a mixed-mode of normal faulting and dike intrusion.

Discussion: The growth of pit craters above dikes and the increase in pit crater diameter with increasing dike top depth is well documented from field observations and numerical models [10]. Further, dike propagation along preexisting faults has been observed on Earth [11] and inferred in Valles Marineris [12]. Motivated by these observations, we propose the following interpretation of dike-related pit crater chain growth in northern Valles Marineris (Fig. 4). Below pit crater chains characterized by normal fault topographies and blunt terminations, the causative dike propagated along preexisting normal faults at sufficient depth to have negligible effect on the preexisting fault-related topography. This dike promoted stoping by increasing opening mode displacements along the preexisting fault. Toward the mid-sections the pit crater chains, the dike top depth is inferred to be shallower (but still following a preexisting normal fault), thereby contributing a larger component of dike-related deformation to an effective mixed-mode pit crater chain topography. At and beyond the tapering end of the pit crater chains, the dike top depth is shallowest and the dike has propagated past the preexisting normal fault, resulting in a purely dike-related topography.

Geologic mapping has established that normal faulting related to the growth of Valles Marineris occurred during the Hesperian, and that the pit crater chains studied here formed subsequently during the Late Hesperian to Early Amazonian [13]. Therefore we propose that during the Late Hesperian to Early Amazonian, Tharsis-radial dikes propagated along preexisting Hesperian-aged normal faults related to the formation of Valles Marineris. These dikes are confined to the north of the Ius–Melas–Coprates chasmata. The timing and location of these dikes supports interpretations of a volcanic origin for the interior layered deposits [15], by documenting a potential magma transport mechanism for these eruptions.

Propagation of these causative dikes indicate that the stress state at Valles Marineris during the Late Hesperian to Early Amazonian was dominated by Tharsis-radial compressive stresses that were equal in magnitude or greater than lithostatic load. Also, the Tharsis-concentric stress magnitude was less than either the Tharsis-radial stress or lithostatic load. In order for dikes to propagate along a preexisting fault, the orientation of each principal stress at the time of dike propagation must be sub-parallel with their respective orientations at the time of faulting [16], implying negligible net stress rotation between periods of normal faulting and pit crater chain formation. We therefore find that the stress states during both periods of activity are consistent with geodynamic models of lithospheric flexure by Tharsis loading [e.g. 2].

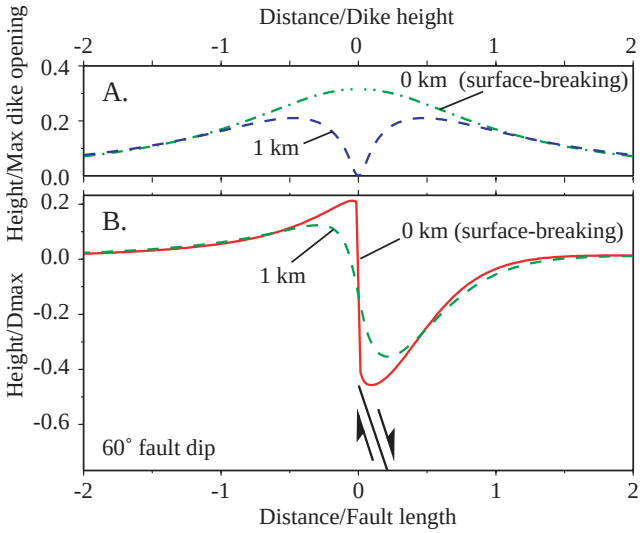

Figure 2. Above. Numerical model predictions of surface topography above A) dikes and B) normal faults at the labeled upper tip depths.

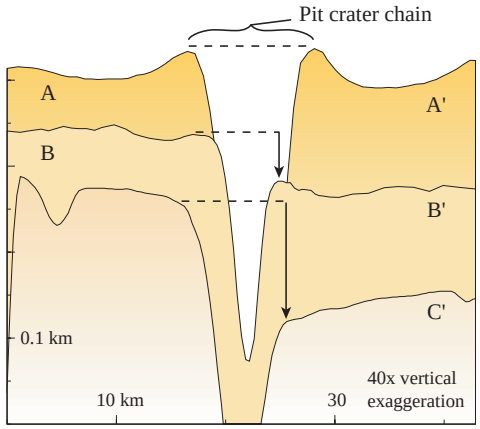

Figure 3. Right. MOLA-based profiles showing A–A') dike, B–B') mixed-mode, and C–C') normal fault topography. Profile locations shown in Figure 1.

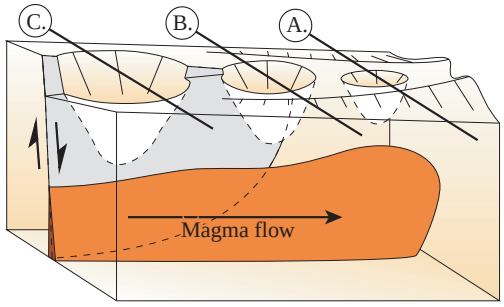

Figure 4. Interpretation of along-strike changes in A) dike, B) mixed-mode, and C) normal fault topography.

References: [1] Tanaka and Golombek, (1989) *Proc. LPSC* 19th, 383–396. [2] Banerdt et al., (1992) in *Mars*, 249–297, Univ. Ariz. Press. [3] Davis et al., (1995) *Icarus*, 114, 403–422. [4] Mège et al (2003) *J. Geophys. Res*., 2002JE001852. [5] Wyrick et al., (2004) *J. Geophys. Res*., 2004JE002240. [6] Ferrill et al., (2004) *GSA Today*, 14, 4–12. [7] Schultz, (1992) *Eng. Anal. Bound. Elem.*, 10, 147–154. [8] Schultz et al., (2004) *Geology*, 32, 889–892. [9] Okubo and Schultz, (2004) *Comp. Geosci*., 30, 59–72. [10] Okubo and Martel (1998), *J. Volcanol. Geotherm. Res*., 86, 1–18. [11] Tilling et al., (1987) *USGS Prof. Pap. 1350*, 405–469. [12] Luchitta, (1987) *Science*, 30, 565–567. [13] Tanaka et al., (1991) *J. Geophys. Res*., 96, 15617–15633., [14] Anderson et al, (2001) *J. Geophys. Res*., 106, 20563–20585. [15] Luchitta, (1990) *Icarus*, 86, 476–509. [16] Ziv et al., (2000) *J. Geophys. Res*., 105, 5947–5961.

Abstract published in: Lunar and Planetary Science XXXVI, CD-ROM, Lunar and Planetary Institute, Houston (2005).